
Self-Correcting VLA: Online Action Refinement via Sparse World Imagination

Chenyv Liu^{1*} Wentao Tan^{1*} Lei Zhu¹✉ Fengling Li² Jingjing Li³ Guoli Yang⁴ Heng Tao Shen¹

Abstract

Standard vision-language-action (VLA) models rely on fitting statistical data priors, limiting their robust understanding of underlying physical dynamics. Reinforcement learning enhances physical grounding through exploration yet typically relies on external reward signals that remain isolated from the agent’s internal states. World action models have emerged as a promising paradigm that integrates imagination and control to enable predictive planning. However, they rely on implicit context modeling, lacking explicit mechanisms for self-improvement. To solve these problems, we propose Self-Correcting VLA (SC-VLA), which achieve self-improvement by intrinsically guiding action refinement through sparse imagination. We first design sparse world imagination by integrating auxiliary predictive heads to forecast current task progress and future trajectory trends, thereby constraining the policy to encode short-term physical evolution. Then we introduce the online action refinement module to reshape progress-dependent dense rewards, adjusting trajectory orientation based on the predicted sparse future states. Evaluations on challenging robot manipulation tasks from simulation benchmarks and real-world settings demonstrate that SC-VLA achieve state-of-the-art performance, yielding the highest task throughput with **16%** fewer steps and a **9%** higher success rate than the best-performing baselines, alongside a **14%** gain in real-world experiments. Code is available at <https://github.com/Kisaragi0/SC-VLA>.

1. Introduction

Vision-language-action models (VLA) have driven recent advancements in embodied AI by bringing multimodal large

^{*}Equal contribution ¹Tongji University ²University of Technology Sydney ³University of Electronic Science and Technology of China ⁴Advanced Institute of Big Data. Correspondence to: Lei Zhu <leizhu0608@gmail.com>.

Preprint Version.

language models (MLLMs) to physical control (Zitkovich et al., 2023; Driess et al., 2023; Kim et al., 2024; Team et al., 2024). By performing large-scale imitation learning on diverse robotic datasets, these architectures enable agents to translate natural language instructions directly into executable actions. However, this paradigm fundamentally relies on fitting the statistical patterns inherent in the pre-training data. Consequently, the learned policies mainly depend on memorized data priors rather than acquiring a robust understanding of the underlying physical dynamics (Chow et al., 2025; Zheng et al., 2024).

To address the reliance on static priors, reinforcement learning introduces active interaction into the training process. Instead of passively cloning expert behaviors, agents optimize their policies by exploring the environment and learning from rewards. To implement this, several research paradigms have emerged. A prominent strategy employs online reinforcement learning algorithms, such as PPO (Schulman et al., 2017), to fine-tune pre-trained VLA for task-specific adaptation (Liu et al., 2025; Lu et al., 2025). Alternatively, offline reinforcement learning methods seek to extract optimal policies from static datasets, enhancing performance without necessitating real-time interaction (Kumar et al., 2020; Chebotar et al., 2023). However, effective learning relies on the quality of feedback signals, which are often difficult to define manually for diverse tasks and scenarios. To address this, recent methods incorporate multimodal large language models to synthesize reward functions, using semantic reasoning to guide policy optimization (Lu et al., 2025; Zhai et al., 2025). Despite these advancements, a critical limitation persists: *whether manually defined or synthesized by models, these approaches typically rely on external reward signals to evaluate performance*. This reliance can introduce a disconnect between the external signals and the model’s internal states. Therefore, it is essential to explore efficient self-improvement strategies that facilitate the model’s native adaptation capabilities.

To bridge this gap, world models offer a promising direction by establishing internal physical dynamics. However, current reinforcement learning algorithms for VLA typically treat world models and policies as independent modules, relying on closed-loop feedback for exploration (Hung et al., 2025). This separation overlooks the unique capability of another paradigm, termed **world action models** (Wu et al.,

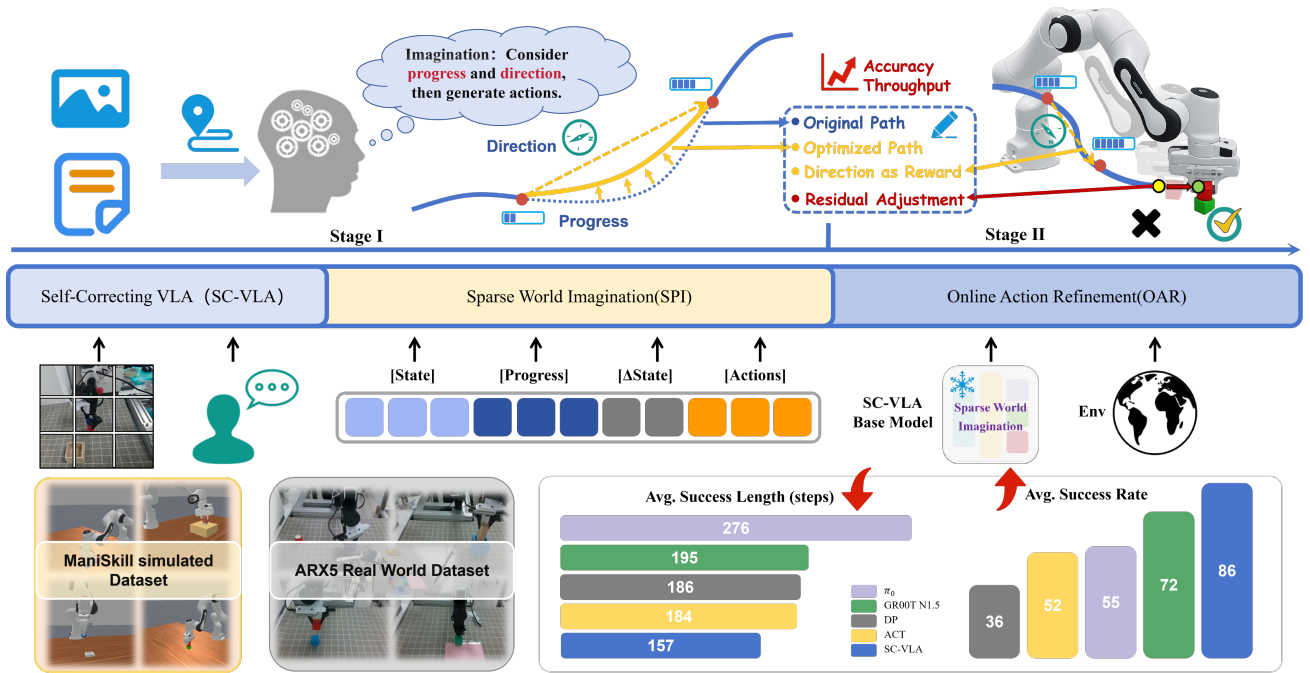


Figure 1. We present Self-Correcting VLA (SC-VLA), a novel framework designed to enhance physical grounding through intrinsic self-improvement. The model is equipped with Sparse World Imagination (SPI) to forecast task progress and future trajectory trends, and Online Action Refinement (OAR) to dynamically optimize policies via residual adjustments and reshaped rewards. SC-VLA achieves superior performance on ManiSkill and real-world ARX5 benchmarks, surpassing baselines in both success rate and execution throughput.

2023; Zhao et al., 2025; Black et al., 2023), which natively support both action generation and multimodal future prediction. While this allows intrinsic evaluation via predicted future states, existing approaches lack explicit mechanisms to leverage these states to refine actions, failing to realize self-improvement aligned with the agent’s internal states.

To achieve self-improvement by intrinsically guiding action refinement through future imagination, we propose Self-Correcting VLA (SC-VLA). This framework jointly generates actions while predicting sparse future states, enabling fine-grained trajectory refinement via residual reinforcement learning for complex manipulation tasks. SC-VLA significantly enhances task success rate and throughput. Specifically, we introduce sparse world imagination, which integrates auxiliary predictive heads to forecast current task progress and future trajectory orientation as sparse world signals. This mechanism constrains the policy to encode short-term physical evolution prior to action generation. Based on this, we further propose online action refinement, which constructs dense rewards by evaluating the consistency between the current and future trajectory orientation. It employs imagination to deduce future action trends for reshaping intrinsic progress-dependent dense rewards, thereby eliminating reliance on external reward models. We evaluate our method on four challenging manipulation tasks (StackCube, PlaceSphere, LiftPegUpright, and PegInsertion), where SC-VLA demonstrates state-of-the-art

performance with the highest task throughput.

- We propose SC-VLA, a self-correcting framework that integrates offline action generation with online refinement. By introducing sparse world imagination to forecast sparse future states, it constrains the policy to encode physical evolution.
- We develop online action refinement with residual reinforcement learning to adjust trajectory orientation. It constructs progress-dependent dense rewards using predicted future states, explicitly guiding the policy to align with the imagined future behavioral trends.
- We conduct systematic evaluations on four tasks across both simulation and real-world robotic platform. The results demonstrate that SC-VLA achieves the best performance in task throughput and success rate on complex manipulation tasks.

2. Related Works

Vision-Language-Action Models. Vision-Language-Action (VLA) models integrate multimodal models into robotic control (Brohan et al., 2022; Li et al., 2023; Liu et al., 2024). RT-2 (Zitkovich et al., 2023) enables semantic transfer by modeling actions as discrete tokens, while OpenVLA (Kim et al., 2024) enhances cross-robot

generalization through efficient adaptation. Recently, GROOT (Bjorck et al., 2025) and π_0 (Black et al., 2024) have improved real-time deployment and continuous action generation via dual-system architectures and flow matching, respectively. Despite these advances, existing methods rely heavily on offline imitation and current-step semantic alignment, lacking explicit modeling of physical evolution.

Reinforcement Learning for VLA. The key to introducing reinforcement learning into pretrained VLA models lies in constructing effective external rewards to alleviate the sparse feedback problem. Existing approaches can be broadly categorized into three classes. The first class leverages the semantic reasoning capability of vision-language models (VLM) to directly evaluate execution processes or diagnose failure causes, thereby synthesizing trajectory-level rewards or corrective signals, such as VLA-RL (Lu et al., 2025), VLAC (Zhai et al., 2025), Reflective Self-Adaptation (Li et al., 2025a), and World-Env (Xiao et al., 2025), which provide high-level semantic guidance through language understanding and causal reasoning. The second class designs rewards via explicit rules or auxiliary prediction objectives, including rule-based signals derived from remaining steps or temporal information (e.g., Self-Improving (Ghasemipour et al., 2025), $\pi_{0.6}^*$ (Intelligence et al., 2025), and RFTF (Shu et al., 2025)), as well as approaches such as NORA-1.5 (Hung et al., 2025) that evaluate trajectory deviations using action-conditioned world models. The third class constructs rewards based on feature or trajectory similarity metrics, typically by comparing generated trajectories with target trajectories in pixel, perceptual, or latent feature spaces, as exemplified by ThinkAct (Huang et al., 2025) and VLA-RFT (Li et al., 2025b). Despite significantly improving exploration efficiency, these methods generally rely on external model inference, handcrafted rules, or similarity computations, which are decoupled from the policy’s internal representations and introduce additional computational and system complexity. In contrast, approaches that rely solely on scalar return prediction (e.g., ReinboT (Zhang et al., 2025)) struggle to provide fine-grained spatiotemporal geometric constraints.

World Action Models. Unlike RL-based VLA methods that rely on external reward signals, world action models aim to jointly model action generation and future evolution within a unified framework, constraining policy behavior via latent contextual predictions and thereby enabling intrinsic guidance without explicit external rewards. GR-MG (Li et al., 2025c) conditions current actions on imagined future target images by generating pixel-level goals. FLARE (Zheng et al., 2025) further avoids high-dimensional pixel synthesis by aligning future representations in latent space, improving both efficiency and stability. PAR (Song et al., 2025) proposes a physics-aware autore-

gressive modeling paradigm that unifies vision and actions as continuous physical tokens, directly leveraging dynamical priors from video models for control. WorldVLA (Cen et al., 2025) alternates between predicting actions and future visual states in an autoregressive manner, mitigating error accumulation through attention masking and achieving mutual reinforcement between action generation and world modeling. Despite their ability to constrain policies with predictive latent context, the future signals in these approaches are typically encoded as implicit representations, lacking interpretable physical semantics or explicit self-evaluation mechanisms. As a result, they struggle to perform fine-grained corrections on short-horizon trajectories and cannot provide direct policy improvement signals in the same manner as reward-based paradigms.

3. Preliminary

3.1. Basic Robot Policy

To address the multimodal distribution inherent in robot action generation, we adopt Flow Matching (FM) as the backbone of our policy. Compared to diffusion-based models, flow matching constructs deterministic optimal transport paths, significantly improving training efficiency and inference stability while preserving generation quality.

Concretely, given an observation o , conditional flow matching aims to learn an observation-conditioned vector field v_θ that continuously transforms samples from a prior noise distribution $p_0(x) = \mathcal{N}(x | 0, I)$ into a target action distribution $p_1(x) \approx q(a | o)$. During training, we construct an optimal transport interpolation path

$$x_t = tx_1 + (1 - t)x_0, \quad (1)$$

which connects a noise sample $x_0 \sim p_0$ and a ground-truth action sample $x_1 \sim q(a | o)$. The corresponding target velocity field is given by $x_1 - x_0$. The model parameters are optimized by minimizing the mean squared error between the predicted vector field and the target velocity field:

$$\mathcal{L}_{\text{FM}}(\theta) = \mathbb{E}_{t, x_0, x_1, o} \left[\|v_\theta(x_t, t, o) - (x_1 - x_0)\|_2^2 \right]. \quad (2)$$

At inference time, the model starts from a prior noise sample and generates the final action by solving the corresponding ordinary differential equation (ODE) with a numerical integrator (e.g., Euler stepping):

$$x_1 = x_0 + \int_0^1 v_\theta(x_t, t, o) dt. \quad (3)$$

In the following sections, we build upon this conditional flow matching formulation and introduce additional structured predictive constraints to enhance the policy’s ability to model short-term physical evolution.

3.2. Soft Actor-Critic (SAC)

To enable stable and efficient policy optimization in continuous action spaces, we adopt Soft Actor-Critic (SAC) (Haarnoja et al., 2018) as the underlying reinforcement learning algorithm. SAC is an off-policy method based on the maximum entropy reinforcement learning framework, which augments the expected return objective with an entropy regularization term. This formulation encourages a balance between exploration and exploitation, leading to improved stability and robustness of the learned policy. The optimization objective of SAC is defined as:

$$J(\pi) = \mathbb{E}_{\tau \sim \pi} \left[\sum_{t=0}^{\infty} \gamma^t (r(s_t, a_t) + \alpha \mathcal{H}(\pi(\cdot | s_t))) \right], \quad (4)$$

where $\mathcal{H}(\pi(\cdot | s_t))$ denotes the entropy of the policy at state s_t , and α is an automatically tuned temperature parameter that controls the strength of entropy regularization.

In continuous action spaces, SAC typically updates the policy using the reparameterization trick, in which action sampling is expressed as

$$a_t = f_{\theta}(s_t, \xi), \quad \xi \sim \mathcal{N}(0, I), \quad (5)$$

enabling low-variance gradient backpropagation through the stochastic policy.

4. Self-Correcting VLA

We present Self-Correcting VLA (SC-VLA), a two-stage framework illustrated in Fig. 2. SC-VLA integrates sparse world imagination (SPI) with residual reinforcement learning for online action refinement (OAR). Crucially, the reward signals are **endogenous**, derived purely from the internal consistency of world imagination rather than external dense supervision. This design comprises two key components: (i) a flow-matching base policy guided by sparse imagination (Sec. 4.1), and (ii) a residual module optimized via intrinsic predictive rewards (Sec. 4.2).

4.1. Sparse World Imagination

Conditional Information Processing. We leverage a Vision-Language Model (VLM) to fuse multimodal observations into a unified representation. Specifically, multi-view images I_k are encoded by the SigLIP-2 (Tschannen et al., 2025) backbone and concatenated with the language instruction \mathcal{L} . This joint sequence is then processed by Eagle-2 (Li et al., 2024). To balance high-level semantic understanding with low-level control features, we extract the hidden states from an intermediate layer l as the conditioning signal \mathbf{o}_{mid} :

$$\mathbf{o}_{\text{mid}} = \Phi_{\text{VLM}}^{(l)}(\mathcal{E}_{\text{vis}}(I_k), \mathcal{L}), \quad (6)$$

where \mathcal{E}_{vis} denotes the SigLIP-2 encoder and $\Phi_{\text{VLM}}^{(l)}$ represents the VLM backbone truncated at layer l .

Query Sequence Construction. To compensate for the lack of physical consistency constraints in standard flow matching, we introduce a physics regularization mechanism based on sparse world imagination. Explicit world prediction targets are injected into the query sequence to be jointly modeled with the action vector field. The augmented input query sequence is defined as:

$$\mathbf{q}_{\text{input}} = [\mathbf{s}_t, \mathbf{q}_{p_t}, \mathbf{q}_{\Delta s_t}, \mathbf{q}_a]. \quad (7)$$

Here, $\mathbf{s}_t \in \mathbb{R}^{1 \times D}$ denotes the current embodiment state, and $\mathbf{q}_a \in \mathbb{R}^{16 \times D}$ corresponds to the queries for action trajectory generation. These two components serve as the base queries for action generation. $\mathbf{q}_{p_t} \in \mathbb{R}^{1 \times D}$ is used to predict the task progress p_t , providing the model with explicit temporal evolution cues. $\mathbf{q}_{\Delta s_t} \in \mathbb{R}^{1 \times D}$ is introduced to model short-horizon future physical state variations, capturing the spatial displacement trends induced by the action. Specifically, we model short-term physical evolution as a relative transformation within the current local coordinate frame. We define the target state at a future time step $t' = t + H + \delta$, where H is the execution horizon and $\delta \sim \mathcal{U}(-\Delta, \Delta)$ is a random temporal offset introduced for robustness. The relative state increment $\Delta s_t \in \mathbb{R}^7$ is calculated as:

$$\Delta s_t = [R_t^\top (P_{t'} - P_t), \text{Euler}(R_t^\top R_{t'}), g_{t'} - g_t]. \quad (8)$$

Here, $P \in \mathbb{R}^3$, $R \in SO(3)$, and $g \in \mathbb{R}$ denote the end-effector position, rotation matrix, and gripper opening, respectively. The operator $\text{Euler}(\cdot)$ extracts Euler angles from the relative rotation matrix. This sparse, local-frame prediction objective enhances the model’s generalization to physical dynamics across varying temporal scales.

Joint Optimization. In the DiT backbone composed of N Transformer blocks, the final block primarily focuses on modeling the action distribution, while intermediate layers retain explicit representations of the world state. To encode short-term physical evolution prior to action generation, we extract the hidden representation $h^{(m)}$ from the m -th intermediate block. Based on this feature, we predict the task progress p_t and relative state change Δs_t using independent lightweight MLP heads:

$$\hat{p}_t = f_{\text{prog}}(h_{p_t}^{(m)}), \quad \widehat{\Delta s}_t = f_{\Delta s_t}(h_{\Delta s_t}^{(m)}). \quad (9)$$

We jointly optimize the flow matching objective with this auxiliary physical supervision. The overall training objective is defined as:

$$\mathcal{L}_{\text{total}} = \mathcal{L}_{\text{FM}} + \lambda_1 \mathcal{L}_{\text{prog}} + \lambda_2 \mathcal{L}_{\Delta s_t}, \quad (10)$$

where $\mathcal{L}_{\text{prog}}$ and $\mathcal{L}_{\Delta s_t}$ are supervised using Mean Squared Error (MSE), weighted by coefficients λ_1 and λ_2 . Through

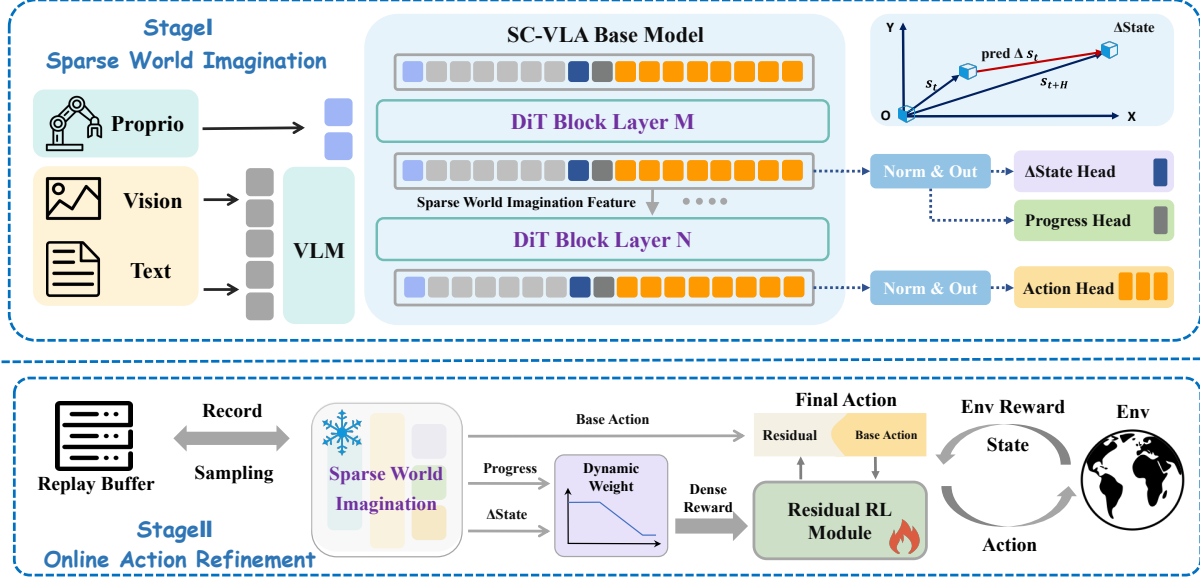


Figure 2. The architecture of Self-Correcting VLA. The framework consists of two stages: Stage I (Top) utilizes a VLM and DiT-based backbone to generate base actions and sparse world imagination, decoded from the final output (Layer N) and intermediate features (Layer M), respectively. Stage II (Bottom) implements Online Action Refinement, where a Residual RL Module optimizes the final action by learning a residual term. This process is guided by endogenous dense rewards derived from the dynamic weighting of imagination consistency (Progress and Δ State) without external supervision.

this joint optimization, the model not only learns to generate precise actions but also internalizes a coherent and interpretable sparse world representation within $h^{(m)}$, providing robust guidance for the subsequent residual policy adaptation.

4.2. Online Action Refinement

While the base policy (Sec. 4.1) enhances stability by encoding physical evolution, it remains limited by offline data, often struggling with out-of-distribution perturbations and fine-grained contacts. To address this without learning from scratch, we introduce a residual RL module atop the base priors. This module performs minimal online corrections to base actions, enabling effective adaptation in high-precision settings.

Residual Policy. To balance the stability of the base policy and online adaptability to environmental perturbations, we adopt a residual policy structure. The input space of the residual policy π_{res} is reconstructed as a *sparse world imagination observation* $o_w \in \mathbb{R}^{16}$:

$$o_w = (s_t, \hat{p}_t, \widehat{\Delta} s_t). \quad (11)$$

In this work, we follow the Policy Decorator (Yuan et al., 2024) to model the residual policy π_{res} as a Gaussian policy parameterized by a lightweight multilayer perceptron (MLP) and adopt the Soft Actor-Critic (SAC) (Haarnoja et al., 2018)

algorithm because it has excellent sample efficiency and stability. The final action a_t is jointly determined by a frozen base policy $a_t^{\text{base}} \sim \pi_{\text{base}}(o_{\text{mid}})$ and a learnable residual policy $a_t^{\text{res}} \sim \pi_{\text{res}}(o_w)$:

$$a_t = a_t^{\text{base}} + \lambda a_t^{\text{res}}, \quad (12)$$

where λ is a residual scaling coefficient. By explicitly incorporating task progress and state evolution predicted by the first-stage model, the residual network can perceive the intent of the base policy. This design enables the residual policy to perform local adjustments around the physical evolution priors provided by the model, thereby avoiding inefficient and unconstrained exploration in the raw observation space.

Dense Reward Mechanism. Although the residual architecture reduces the dimensionality of exploration, the environment reward remains highly sparse. To address this issue, we construct a directional dense guidance reward using the short-term state change $\widehat{\Delta} s_t$ predicted by the base policy. Specifically, we extract only the first three translational components $\Delta s_t^{\text{pos}} \in \mathbb{R}^3$ from Δs_t and define the short-term goal position at the current timestep as

$$P_{\text{goal}} = P_t + \widehat{\Delta} s_t^{\text{pos}}. \quad (13)$$

After executing the residual action, the guidance reward is computed based on the alignment between the actual end-

effector displacement and the predicted evolution direction:

$$r_t^{\text{guide}} = \frac{(P_{t+n} - P_t) \cdot (P_{\text{goal}} - P_t)}{\|P_{t+n} - P_t\| \|P_{\text{goal}} - P_t\| + \epsilon}. \quad (14)$$

Here, P_{t+n} denotes the end-effector position after executing the action for n steps ($n < H$). This reward provides continuous directional feedback at each step, guiding the residual policy to perform local adjustments along the short-term physical evolution direction predicted by the base policy, thereby effectively alleviating exploration difficulties under sparse reward settings.

Algorithm 1 SC-VLA: Online Action Refinement

- 1: **Input:** Frozen SC-VLA base policy π_{base} , online action refinement policy π_{res} , environment Env
 - 2: Initialize replay buffer \mathcal{D}
 - 3: Initialize total training steps T_{train}
 - 4: $t \leftarrow 0$
 - 5: **while** $t < T_{\text{train}}$ **do**
 - 6: Observe state s_t
 - 7: Query base policy: $(a_t^{\text{base}}, \hat{p}_t, \widehat{\Delta s}_t) \sim \pi_{\text{base}}(o_{\text{mid}})$
 - 8: Construct augmented observation o_w^t by Eq. (11)
 - 9: Sample residual action $a_t^{\text{res}} \sim \pi_{\text{res}}(o_w^t)$
 - 10: Execute action $a_t \leftarrow a_t^{\text{base}} + \lambda a_t^{\text{res}}$
 - 11: Step environment: $(o_w^{t+1}, r_t^{\text{env}}) \leftarrow \text{Env.Step}(a_t)$
 - 12: Compute final reward r_t^{final} by Eq. (15)
 - 13: Add $(o_w^t, a_t^{\text{base}}, a_t^{\text{res}}, o_w^{t+1}, a_{t+1}^{\text{base}}, r_t^{\text{final}})$ in \mathcal{D}
 - 14: Update π_{res} and critics using SAC
 - 15: $t \leftarrow t + 1$
 - 16: **end while**
-

Dynamic Weight Scheduling. While sparse world imagination accelerates global exploration, a static predictive prior may limit the policy’s optimization capability during fine-grained contact phases due to distribution shift. To address this issue, we propose a *dynamic weight scheduling*. Specifically, we use the predicted task progress \hat{p}_t as a scheduling signal, allowing predictive guidance to dominate in the early stages of the task and to be gradually weakened in later stages, thereby enabling a smooth transition from predictive-prior guidance to autonomous exploration. The final reward is defined as a weighted combination of the environment reward and the predictive guidance reward:

$$r_t^{\text{final}} = \eta(\hat{p}_t) \cdot w_{\text{guide}} \cdot r_t^{\text{guide}} + r_t^{\text{env}} - c, \quad (15)$$

where $\eta(\cdot)$ is a monotonically decreasing scheduling function with respect to task progress, w_{guide} is the guidance weight, r_t^{env} denotes the sparse environment reward, and c is a per-step time penalty. This mechanism effectively balances early exploration efficiency and late-stage sensitivity to real dynamics feedback, ensuring stable convergence of the policy during the fine-tuning phase.

5. Experiments

In this section, we systematically evaluate the effectiveness of *Self-Correcting Vision-Language-Action* (SC-VLA) through both simulation and real-robot experiments, with a primary focus on success rate, throughput and transferability in complex manipulation tasks. Specifically, our experimental analysis is organized around the following key questions:

1. Can SC-VLA improve the success rate of flow-matching policies in complex manipulation tasks through sparse world imagination combined with a residual module?
2. Can the dense reward constructed based on sparse world imagination and the dynamic weight scheduling alleviate the issue of low exploration efficiency caused by sparse rewards and improve policy throughput?
3. What are the respective contributions of the key components in the proposed framework to the overall performance?
4. Can the proposed method be stably transferred to real robotic systems and maintain robustness under environmental perturbations?

5.1. Simulation Setup and Baselines

ManiSkill3. We evaluate our method on ManiSkill3 (Tao et al., 2024), a SAPIEN-based (Xiang et al., 2020) platform offering high-fidelity contact dynamics suitable for complex manipulation. We select four challenging tasks: *StackCube*, *PlaceSphere*, *PegInsertion*, and *LiftPegUpright*, to cover capabilities ranging from precise pick-and-place to non-prehensile manipulation. For fair comparison, all methods are trained with 100 demonstrations per task and evaluated over 50 episodes. See Appendix A for details.

Baselines. We compare SC-VLA against baselines representing mainstream paradigms: *Diffusion Policy* (DP) (Chi et al., 2025) for diffusion-based control, *ACT* (Zhao et al., 2023) for action chunking, and π_0 (Black et al., 2024) for flow-matching policies, alongside our base model GROOT N1.5 (Bjorck et al., 2025). We use task success rate as the primary metric. Additionally, we report average episode length during the RL stage to evaluate exploration efficiency and system throughput. Detailed configurations are provided in Appendix B.

Quantitative Results. Table 1 summarizes the success rates of all methods on four challenging manipulation tasks in ManiSkill. Overall, the proposed *Self-Correcting Vision-Language-Action* method demonstrates superior performance, significantly outperforming existing baseline approaches across all categories. Taking the most challenging

Table 1. Success rates of all methods in ManiSkill. Due to the absence of language guidance in DP, ACT, we evaluate them under two settings: ‡ denotes a single multi-task policy trained on all tasks simultaneously. † denotes training independent specialist models for each of the four tasks separately.

Model	ManiSkill Tasks				Avg
	Stack Cube	Place Sphere	LiftPeg Upright	Peg Insertion	
DP‡	0.46	0.90	0.10	0.00	0.36
DP†	<u>0.88</u>	<u>1.00</u>	<u>0.80</u>	<u>0.40</u>	<u>0.77</u>
ACT‡	0.50	0.88	0.60	0.12	0.52
ACT†	0.64	0.90	0.46	0.04	0.51
π_0	0.66	0.86	0.48	0.22	0.55
GR00T N1.5	0.78	<u>1.00</u>	0.72	<u>0.40</u>	0.72
SC-VLA(SPI)	0.96	1.00	0.82	0.50	0.82
SC-VLA(SPI, OAR)	1.00	1.00	0.88	0.56	0.86
Δ from OAR	+4%	+0%	+6%	+6%	+4%

Table 2. Average completion length over successful episodes.

Model	ManiSkill Tasks				Avg
	Stack Cube	Place Sphere	LiftPeg Upright	Peg Insertion	
DP‡	162	146	202	800	327
DP†	132	125	<u>197</u>	233	<u>172</u>
ACT‡	<u>148</u>	131	207	250	184
ACT†	198	126	203	<u>230</u>	189
π_0	265	179	331	331	276
GR00T N1.5	192	<u>122</u>	209	257	195
SC-VLA(SPI)	169	128	190	262	187
SC-VLA(SPI,OAR)	158	110	189	173	157
Δ from OAR	↓ 6.2%	↓ 14.0%	↓ 0.5%	↓ 34.0%	↓ 16.0%

PegInsertion task as an example, SC-VLA (SPI) improves the success rate by **28%** and **10%** over pretrained models such as π_0 (Black et al., 2024) and GR00T N1.5 (Bjorck et al., 2025), respectively, demonstrating that explicitly incorporating short-horizon physical state prediction effectively enhances control precision in complex contact scenarios. Building on this, the introduction of residual reinforcement learning further boosts the performance, with SC-VLA (SPI, OAR) achieving an average success rate of 86%.

In addition, Table 2 reports the average completion length over **successful episodes** for all methods. SC-VLA attains the shortest average completion length of 157 steps, indicating the highest execution efficiency. This corresponds to a **43%** reduction compared to pretrained models such as π_0 (Black et al., 2024), and a **8%** reduction relative to lightweight policies such as Diffusion Policy (DP) (Chi et al., 2025). These results show that the proposed method achieves both more precise execution and higher throughput on complex manipulation tasks.

5.2. Ablation Study

To analyze the contribution of each key component in the SC-VLA framework, we conduct a systematic ablation study on the ManiSkill benchmark. All ablation variants are trained using the same demonstration data and evaluated under identical protocols, with the average success rate across the four tasks serving as the primary metric to ensure comparability and fairness.

Table 3. Ablation study on different imagination components.

Model	ManiSkill Tasks				Avg
	Stack Cube	Place Sphere	LiftPeg Upright	Peg Insertion	
SC-VLA w/o state	0.88	1.00	0.84	0.42	0.78
SC-VLA w/o prog	0.92	1.00	0.80	0.50	0.80
SC-VLA w/o state_prog	0.78	1.00	0.72	0.40	0.72
SC-VLA(SPI)	0.96	1.00	0.82	0.50	0.82

Effectiveness of Progress Guidance. The progress token (\mathbf{q}_{p_t}) provides explicit temporal progression information for action generation. To evaluate its effectiveness, we conduct an ablation study by removing \mathbf{q}_{p_t} from the query sequence. As shown in Table 3, removing \mathbf{q}_{p_t} reduces the average success rate from 82% to 80%, with the degradation mainly observed on tasks with clear execution stages, such as *StackCube* (96% \rightarrow 92%) and *LiftPegUpright* (82% \rightarrow 80%). These results indicate that the absence of q_{p_t} does not significantly compromise action reliability, but plays an important role in improving the temporal consistency of the policy during multi-stage execution.

Effectiveness of State Guidance. Relative state change modeling (Δs_t) provides directional constraints on short-term physical evolution for action generation. To evaluate its effectiveness, we conduct an ablation study by removing $\mathbf{q}_{\Delta s_t}$ from the query sequence. As shown in Table 3, removing $\mathbf{q}_{\Delta s_t}$ leads to a clear drop in the average success rate from 82% to 78%, with the most pronounced degradation observed in difficult tasks such as *PegInsertion* (50% \rightarrow 42%) and *StackCube* (96% \rightarrow 88%). These results indicate that *delta_state* plays a critical role in stabilizing the physical consistency of action execution, particularly in tasks that are sensitive to contact dynamics and pose accuracy.

Complementarity Between Progress and State Guidance.

We further examine the interaction between progress guidance (p_t) and relative state change modeling (Δs_t) by jointly removing both components. As shown in Table 3, eliminating \mathbf{q}_{p_t} and $\mathbf{q}_{\Delta s_t}$ simultaneously causes the average success rate to drop significantly to 72%, which is markedly lower than the performance under either single ablation setting. This result demonstrates that progress guidance and state guidance play complementary roles in the policy.

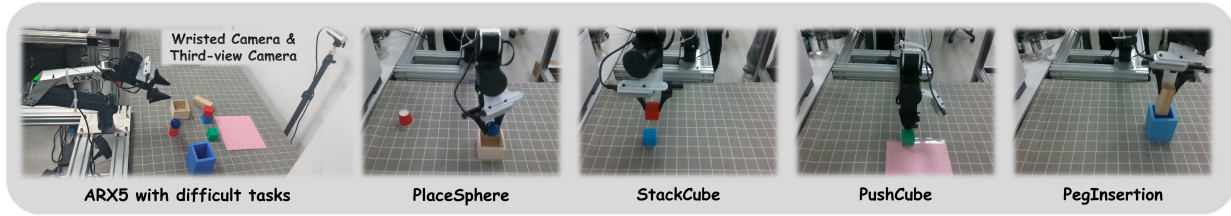


Figure 3. Hardware platforms and visualizations of sampled tasks. The setup is equipped with a wristed camera and a third-person camera.

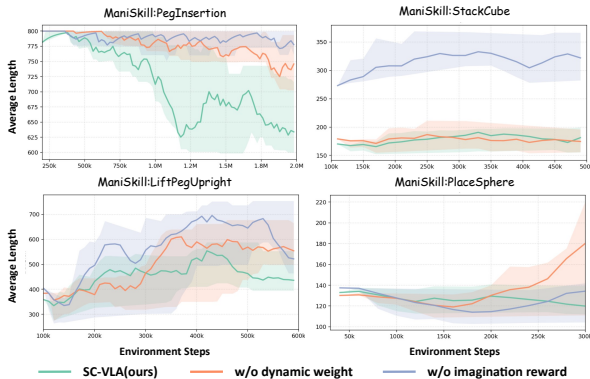


Figure 4. Ablation study on the effectiveness of sparse world imagination rewards and dynamic weight scheduling. We visualize the performance curves starting from the main training phase, excluding the data collection and residual warm-up periods. See Appendix C for further details.

Effectiveness of Sparse World Imagination Rewards.

The sparse world imagination reward plays a pivotal guiding role in reinforcement learning exploration by transforming physical evolution predictions into dense directional feedback. To evaluate its effectiveness, we conducted an ablation study by removing guiding reward and training the residual policy relying solely on the environment’s sparse reward. As shown in Fig. 4, while the performance gap is negligible in the simple *PlaceSphere* task due to the strong base policy, the reward becomes critical in complex tasks like *PegInsertion*. It provides dense feedback to break exploration bottlenecks, reducing average steps from 800 to 650 and boosting throughput. This confirms its essential role in overcoming cold-start problems for complex manipulation.

Effectiveness of Dynamic Weight Scheduling. The dynamic weighting mechanism is responsible for regulating the intensity of prior guidance based on task progress to balance early exploration guidance with later autonomous fine-tuning. To evaluate its effectiveness, we conducted a comparative ablation study by replacing the dynamic decay weight with a fixed constant weight. Results on precision tasks like *PlaceSphere* and *PegInsertion* show that fixed weights lead to significant late-stage degradation, manifesting as divergent step counts or stagnation at sub-optimal

solutions. This highlights the conflict between static priors and fine-grained control, demonstrating that progress-based regulation is essential to prevent prior bias from interfering with fine manipulation.

5.3. Real World Experiments

Setup. We evaluate SC-VLA (SPI) on a real ARX5 arm across four tasks: *StackCube*, *PlaceSphere*, *PegInsertion*, and *PushCube*. Models are trained on 60 demonstrations per task. Hardware setups are visualized in Fig. 3. Given the difficulty of real-world reward design, we benchmark against widely adopted baselines: GR00T N1.5 (Bjorck et al., 2025) and Diffusion Policy (DP) (Chi et al., 2025). We conduct 20 execution trials per task.

Table 4. Success rates on real-world tasks using the ARX5 arm.

Model	Real World Tasks				Avg
	Stack Cube	Place Sphere	Push Cube	Peg Insertion	
DP [‡]	0.30	0.40	0.45	0.00	0.28
GR00T N1.5	0.75	0.45	0.80	0.30	0.57
SC-VLA(SPI)	0.85	0.60	1.00	0.40	0.71

Quantitative Results. As detailed in Table 4, SC-VLA (SPI) demonstrates superior capability, achieving an average success rate of 70% that surpasses DP and GR00T N1.5 by margins of **43%** and **14%**, respectively. Its superior performance in contact-rich tasks, such as *PegInsertion* and *StackCube*, validates that the sparse world imagination effectively enhances robustness and generalization in complex real-world dynamics.

6. Conclusion

We propose *Self-Correcting Vision-Language-Action* (SC-VLA), a framework coupling prediction and control via sparse world imagination. This approach addresses the limitations of static priors and insufficient physical modeling in existing VLA. Our results demonstrate that structured predictive priors can guide physically consistent actions without the complexity of explicit world models. By uni-

fyng world-aware modeling with intrinsic reinforcement learning, SC-VLA eliminates the need for manual reward engineering. Extensive experiments confirm that this self-correcting paradigm substantially improves task throughput, offering a robust direction for developing autonomous, self-evolving robotic systems.

Impact Statement

This paper presents work whose goal is to advance the field of Machine Learning. There are many potential societal consequences of our work, none which we feel must be specifically highlighted here.

References

- Bjorck, J., Castañeda, F., Cherniadev, N., Da, X., Ding, R., Fan, L., Fang, Y., Fox, D., Hu, F., Huang, S., et al. Gr00t n1: An open foundation model for generalist humanoid robots. *arXiv preprint arXiv:2503.14734*, 2025.
- Black, K., Nakamoto, M., Atreya, P., Walke, H., Finn, C., Kumar, A., and Levine, S. Zero-shot robotic manipulation with pretrained image-editing diffusion models. *arXiv preprint arXiv:2310.10639*, 2023.
- Black, K., Brown, N., Driess, D., Esmail, A., Equi, M., Finn, C., Fusai, N., Groom, L., Hausman, K., Ichter, B., et al. π_0 : A vision-language-action flow model for general robot control. *arXiv preprint arXiv:2410.24164*, 2024.
- Brohan, A., Brown, N., Carbajal, J., Chebotar, Y., Dabis, J., Finn, C., Gopalakrishnan, K., Hausman, K., Herzog, A., Hsu, J., et al. Rt-1: Robotics transformer for real-world control at scale. *arXiv preprint arXiv:2212.06817*, 2022.
- Cadene, R., Alibert, S., Soare, A., Gallouedec, Q., Zouitine, A., and Wolf, T. Lerobot: State-of-the-art machine learning for real-world robotics in pytorch, 2024.
- Cen, J., Yu, C., Yuan, H., Jiang, Y., Huang, S., Guo, J., Li, X., Song, Y., Luo, H., Wang, F., et al. Worldvla: Towards autoregressive action world model. *arXiv preprint arXiv:2506.21539*, 2025.
- Chebotar, Y., Vuong, Q., Hausman, K., Xia, F., Lu, Y., Irpan, A., Kumar, A., Yu, T., Herzog, A., Pertsch, K., et al. Q-transformer: Scalable offline reinforcement learning via autoregressive q-functions. In *Conference on Robot Learning*, pp. 3909–3928. PMLR, 2023.
- Chi, C., Xu, Z., Feng, S., Cousineau, E., Du, Y., Burchfiel, B., Tedrake, R., and Song, S. Diffusion policy: Visuomotor policy learning via action diffusion. *The International Journal of Robotics Research*, 44(10-11): 1684–1704, 2025.
- Chow, W., Mao, J., Li, B., Seita, D., Guizilini, V., and Wang, Y. Physbench: Benchmarking and enhancing vision-language models for physical world understanding. *arXiv preprint arXiv:2501.16411*, 2025.
- Driess, D., Xia, F., Sajjadi, M. S., Lynch, C., Chowdhery, A., Wahid, A., Tompson, J., Vuong, Q., Yu, T., Huang, W., et al. Palm-e: An embodied multimodal language model. 2023.
- Ghasemipour, S. K. S., Wahid, A., Tompson, J., Sanketi, P., and Mordatch, I. Self-improving embodied foundation models. *arXiv preprint arXiv:2509.15155*, 2025.
- Haarnoja, T., Zhou, A., Abbeel, P., and Levine, S. Soft actor-critic: Off-policy maximum entropy deep reinforcement learning with a stochastic actor. In *International conference on machine learning*, pp. 1861–1870. Pmlr, 2018.
- Huang, C.-P., Wu, Y.-H., Chen, M.-H., Wang, Y.-C. F., and Yang, F.-E. Thinkact: Vision-language-action reasoning via reinforced visual latent planning. *arXiv preprint arXiv:2507.16815*, 2025.
- Hung, C.-Y., Majumder, N., Deng, H., Renhang, L., Ang, Y., Zadeh, A., Li, C., Herremans, D., Wang, Z., and Poria, S. Nora-1.5: A vision-language-action model trained using world model-and action-based preference rewards. *arXiv preprint arXiv:2511.14659*, 2025.
- Intelligence, P., Amin, A., Aniceto, R., Balakrishna, A., Black, K., Conley, K., Connors, G., Darpinian, J., Dhabalia, K., DiCarlo, J., et al. $\pi_0.6$: a vla that learns from experience. *arXiv preprint arXiv:2511.14759*, 2025.
- Kim, M. J., Pertsch, K., Karamcheti, S., Xiao, T., Balakrishna, A., Nair, S., Rafailov, R., Foster, E., Lam, G., Sanketi, P., et al. Openvla: An open-source vision-language-action model. *arXiv preprint arXiv:2406.09246*, 2024.
- Kumar, A., Zhou, A., Tucker, G., and Levine, S. Conservative q-learning for offline reinforcement learning. *Advances in neural information processing systems*, 33: 1179–1191, 2020.
- Li, B., Wu, D., Yan, Z., Liu, X., Zeng, Z., Li, L., and Zha, H. Reflection-based task adaptation for self-improving vla. *arXiv preprint arXiv:2510.12710*, 2025a.
- Li, H., Ding, P., Suo, R., Wang, Y., Ge, Z., Zang, D., Yu, K., Sun, M., Zhang, H., Wang, D., et al. Vla-rft: Vision-language-action reinforcement fine-tuning with verified rewards in world simulators. *arXiv preprint arXiv:2510.00406*, 2025b.

- Li, P., Wu, H., Huang, Y., Cheang, C., Wang, L., and Kong, T. Gr-mg: Leveraging partially-annotated data via multi-modal goal-conditioned policy. *IEEE Robotics and Automation Letters*, 2025c.
- Li, X., Liu, M., Zhang, H., Yu, C., Xu, J., Wu, H., Cheang, C., Jing, Y., Zhang, W., Liu, H., et al. Vision-language foundation models as effective robot imitators. *arXiv preprint arXiv:2311.01378*, 2023.
- Li, Y., Wei, F., Zhang, C., and Zhang, H. Eagle-2: Faster inference of language models with dynamic draft trees. *arXiv preprint arXiv:2406.16858*, 2024.
- Liu, J., Gao, F., Wei, B., Chen, X., Liao, Q., Wu, Y., Yu, C., and Wang, Y. What can rl bring to vla generalization? an empirical study. *arXiv preprint arXiv:2505.19789*, 2025.
- Liu, S., Wu, L., Li, B., Tan, H., Chen, H., Wang, Z., Xu, K., Su, H., and Zhu, J. Rdt-1b: a diffusion foundation model for bimanual manipulation. *arXiv preprint arXiv:2410.07864*, 2024.
- Lu, G., Guo, W., Zhang, C., Zhou, Y., Jiang, H., Gao, Z., Tang, Y., and Wang, Z. Vla-rl: Towards masterful and general robotic manipulation with scalable reinforcement learning. *arXiv preprint arXiv:2505.18719*, 2025.
- Schulman, J., Wolski, F., Dhariwal, P., Radford, A., and Klimov, O. Proximal policy optimization algorithms. *arXiv preprint arXiv:1707.06347*, 2017.
- Shu, J., Lin, Z., and Wang, Y. Rftf: Reinforcement fine-tuning for embodied agents with temporal feedback. *arXiv preprint arXiv:2505.19767*, 2025.
- Song, Z., Qin, S., Chen, T., Lin, L., and Wang, G. Physical autoregressive model for robotic manipulation without action pretraining. *arXiv preprint arXiv:2508.09822*, 2025.
- Tao, S., Xiang, F., Shukla, A., Qin, Y., Hinrichsen, X., Yuan, X., Bao, C., Lin, X., Liu, Y., Chan, T.-k., et al. Maniskill3: Gpu parallelized robotics simulation and rendering for generalizable embodied ai. *arXiv preprint arXiv:2410.00425*, 2024.
- Team, O. M., Ghosh, D., Walke, H., Pertsch, K., Black, K., Mees, O., Dasari, S., Hejna, J., Kreiman, T., Xu, C., et al. Octo: An open-source generalist robot policy. *arXiv preprint arXiv:2405.12213*, 2024.
- Tschannen, M., Gritsenko, A., Wang, X., Naeem, M. F., Alabdulmohsin, I., Parthasarathy, N., Evans, T., Beyer, L., Xia, Y., Mustafa, B., et al. Siglip 2: Multilingual vision-language encoders with improved semantic understanding, localization, and dense features. *arXiv preprint arXiv:2502.14786*, 2025.
- Wu, H., Jing, Y., Cheang, C., Chen, G., Xu, J., Li, X., Liu, M., Li, H., and Kong, T. Unleashing large-scale video generative pre-training for visual robot manipulation. *arXiv preprint arXiv:2312.13139*, 2023.
- Xiang, F., Qin, Y., Mo, K., Xia, Y., Zhu, H., Liu, F., Liu, M., Jiang, H., Yuan, Y., Wang, H., et al. Sapien: A simulated part-based interactive environment. In *Proceedings of the IEEE/CVF conference on computer vision and pattern recognition*, pp. 11097–11107, 2020.
- Xiao, J., Yang, Y., Chang, X., Chen, R., Xiong, F., Xu, M., Zheng, W.-S., and Zhang, Q. World-env: Leveraging world model as a virtual environment for vla post-training. *arXiv preprint arXiv:2509.24948*, 2025.
- Yuan, X., Mu, T., Tao, S., Fang, Y., Zhang, M., and Su, H. Policy decorator: Model-agnostic online refinement for large policy model. *arXiv preprint arXiv:2412.13630*, 2024.
- Zhai, S., Zhang, Q., Zhang, T., Huang, F., Zhang, H., Zhou, M., Zhang, S., Liu, L., Lin, S., and Pang, J. A vision-language-action-critic model for robotic real-world reinforcement learning. *arXiv preprint arXiv:2509.15937*, 2025.
- Zhang, H., Zhuang, Z., Zhao, H., Ding, P., Lu, H., and Wang, D. Reinbot: Amplifying robot visual-language manipulation with reinforcement learning. *arXiv preprint arXiv:2505.07395*, 2025.
- Zhao, Q., Lu, Y., Kim, M. J., Fu, Z., Zhang, Z., Wu, Y., Li, Z., Ma, Q., Han, S., Finn, C., et al. Cot-vla: Visual chain-of-thought reasoning for vision-language-action models. In *Proceedings of the Computer Vision and Pattern Recognition Conference*, pp. 1702–1713, 2025.
- Zhao, T. Z., Kumar, V., Levine, S., and Finn, C. Learning fine-grained bimanual manipulation with low-cost hardware. *arXiv preprint arXiv:2304.13705*, 2023.
- Zheng, R., Liang, Y., Huang, S., Gao, J., Daumé III, H., Kolobov, A., Huang, F., and Yang, J. Tracevla: Visual trace prompting enhances spatial-temporal awareness for generalist robotic policies. *arXiv preprint arXiv:2412.10345*, 2024.
- Zheng, R., Wang, J., Reed, S., Bjorck, J., Fang, Y., Hu, F., Jang, J., Kundalia, K., Lin, Z., Magne, L., et al. Flare: Robot learning with implicit world modeling. *arXiv preprint arXiv:2505.15659*, 2025.
- Zitkovich, B., Yu, T., Xu, S., Xu, P., Xiao, T., Xia, F., Wu, J., Wohlhart, P., Welker, S., Wahid, A., et al. Rt-2: Vision-language-action models transfer web knowledge to robotic control. In *Conference on Robot Learning*, pp. 2165–2183. PMLR, 2023.

Appendix A: Task Setup and Evaluation Details

This appendix provides supplementary details for the ManiSkill3 (Tao et al., 2024) simulation tasks used in the main paper. All tasks are built upon the SAPIEN (Xiang et al., 2020) physics engine and are designed to evaluate robotic manipulation capabilities under high-precision control requirements and complex contact conditions.

A.1 Task Descriptions

(1) StackCube. Stack the cube on top of the other cube: This task requires the robot to grasp a cube and stably stack it on top of another cube. It primarily evaluates pose accuracy during the grasping and placement phases, as well as execution stability. The task is particularly sensitive to positional errors and end-effector jitter.

(2) PlaceSphere. Pick up the ball and place it in the target position: In this task, the robot is required to grasp a spherical object and place it at a designated target location. Due to the tendency of the sphere to roll during contact, this task imposes stringent requirements on end-effector velocity control and dynamic stability.

(3) LiftPegUpright. Pick up the peg and place it upright: This task requires the robot to grasp one side of a peg and adjust the contact relationship to lift it from a horizontal configuration to an upright pose. During manipulation, relative sliding occurs between the peg and the end-effector. The upright phase demands accurate angle control and pose adjustment, making this task particularly challenging in terms of contact modeling and fine-grained control.

(4) PegInsertion. Pick up the peg and insert it into the container next to the peg: This task requires the robot to precisely insert a peg into a hole with small tolerance. It emphasizes accurate pose alignment and fine-grained adjustments during the contact phase, and serves as a standard benchmark for evaluating high-precision manipulation capabilities.

A.2 Training and Evaluation Settings

For all simulation tasks, all methods are trained using the same amount of demonstration data to ensure a fair comparison. After training, each method is independently evaluated over 50 episodes per task, with task success rate reported as the primary performance metric. Reward definitions follow the official ManiSkill3 (Tao et al., 2024) specifications, and the detailed success criteria for each task are summarized in Table 5.

Table 5. Detailed definitions and success criteria for the four manipulation tasks used in our evaluation.

Tasks	Success Criteria	Max Steps
StackCube	The task is considered successful if the horizontal offset of the red cube relative to the green cube does not exceed the half-diagonal of the cube plus 5 mm, the vertical distance between the centers of the two cubes equals one cube edge length with a tolerance of 5 mm, and the red cube remains stationary and is not grasped by the robot end-effector.	800
PlaceSphere	The task is considered successful if the horizontal offset of the sphere relative to the center of the container does not exceed 5 mm, the vertical position satisfies that the contact point between the bottom of the sphere and the container floor has an error within 5 mm, and the sphere is not grasped by the robot end-effector.	500
LiftPegUpright	The task is considered successful if the peg’s orientation is close to the upright configuration, with a deviation around the vertical axis not exceeding 0.08 rad, and the vertical position of the peg’s center of mass deviates from its half-length by no more than 5 mm.	800
PegInsertionside	The task is considered successful if the tail end of the peg lies within the coordinate frame of the box hole, with an offset along the insertion direction no greater than 2 cm, and offsets along the other two orthogonal directions both smaller than 8 mm.	800

Appendix B: Baseline Details and Settings

This appendix provides brief descriptions of the baseline methods used in the main paper. All baselines are trained and evaluated under the same demonstration data budget and evaluation protocols to ensure a fair comparison.

B.1 DP (Diffusion Policy)

Diffusion Policy (Chi et al., 2025) is an imitation learning approach based on diffusion models, which represents continuous action distributions through a progressive denoising process. By effectively modeling multimodal action behaviors, Diffusion Policy has been widely adopted as a strong baseline for robotic manipulation tasks. For the DP baseline, we utilize the implementation provided by the LeRobot (Cadene et al., 2024) codebase. We configure the policy with an observation history of 2 frames ($n_{\text{obs.steps}} = 2$), a prediction horizon of 16 ($H = 16$), and an execution chunk size of 8 ($n_{\text{action.steps}} = 8$). All models are trained for 200,000 iterations on a single NVIDIA RTX 5090 GPU with a batch size of 64. We apply random cropping with a 90% ratio for data augmentation. All other parameters are set to their default values.

B.2 ACT (Action Chunking with Transformers)

ACT (Zhao et al., 2023) combines Conditional Variational Autoencoders (CVAEs) with Transformer architectures to model action sequences in a chunked manner. This design enables the generation of coherent and smooth action trajectories over long horizons, and has demonstrated stable performance in fine-grained manipulation scenarios. For the ACT baseline, we utilize the implementation provided by the LeRobot (Cadene et al., 2024) codebase. We configure the policy with an observation history of 1 frame ($n_{\text{obs.steps}} = 1$), a prediction horizon of 50 ($H = 50$), and an execution chunk size of 20 ($n_{\text{action.steps}} = 20$). All models are trained for 200,000 iterations on a single NVIDIA RTX 5090 GPU with a batch size of 64. All other parameters are set to their default values.

B.3 π_0

π_0 (Black et al., 2024) is a recently proposed robot foundation model developed by Physical Intelligence, which acquires broad robotic manipulation capabilities through large-scale, multi-task and cross-embodiment training. Built upon a pre-trained vision-language model and augmented with a flow-based action generation module, π_0 (Black et al., 2024) demonstrates strong performance on a wide range of real-world robotic manipulation tasks, including long-horizon and highly dexterous scenarios. For the π_0 baseline, we utilize the official implementation. The model is trained for 50,000 iterations on a single NVIDIA RTX PRO 6000 GPU with a batch size of 32. We employ a cosine decay learning rate schedule, configured with 3,000 warmup steps, a peak learning rate of 2×10^{-5} , and a final learning rate of 1.5×10^{-6} (decaying over 100,000 steps). All other parameters are set to their default values.

B.4 GR00T N1.5

GR00T N1.5 (Bjorck et al., 2025) is a robot manipulation model based on flow matching, which uses the DiT architecture to model continuous action distributions and achieves efficient and stable action generation through vector field learning. This paper extends this method based on its underlying architecture and uses it as a base model. For the GR00T N1.5 baseline, we utilize the official implementation. The model is trained for 50,000 iterations on a single NVIDIA L40 GPU with a batch size of 32. The learning rate is set to 1×10^{-4} . All other parameters are set to their default values.

Appendix C: Experiment Details

Multi-Stage Training Protocol. To ensure the stability of the hybrid architecture, integrating a pre-trained Flow Matching DiT base policy with a randomly initialized SAC residual module, we implement a three-stage training protocol. As illustrated in Fig. 5, the residual weight λ is dynamically adjusted to facilitate a smooth transition from pure imitation to residual reinforcement learning:

1. **Initial Data Collection (Buffer Warm-up):** In the very early stage, the residual weight is held constant at $\lambda = 0$. The agent acts solely using the frozen base policy to collect high-quality demonstration trajectories. This phase is strictly for populating the SAC replay buffer with valid transitions, ensuring the critic has a meaningful state distribution to learn from before any policy updates occur.
2. **Residual Injection (Policy Warm-up):** Once the buffer is sufficiently populated, we enter a linear warm-up phase. The residual weight λ is linearly increased from 0 to the target scaling factor. This gradual injection prevents the noise from the initially random residual policy from catastrophically disrupting the control loop, allowing the RL agent to adapt to the base policy’s dynamics without causing immediate task failure.



Figure 5. **Schematic of the multi-stage training protocol and residual weight schedule.** The training process is divided into three distinct phases to ensure stability: (1) *Buffer Warm-up* for gathering demonstrations, (2) *Residual Injection* for gradually introducing the RL policy, and (3) the *Main Training Phase*. The curve illustrates the evolution of the residual weight λ , transitioning from pure imitation to full residual learning.

3. **Main Training Phase:** Upon reaching the target weight, λ remains fixed (subject to the dynamic weight scheduling described in Sec. 4.2), and the formal training and evaluation begin.

Visualization Rationale. It is important to note that the *Data Collection* and *Residual Injection* phases are transient and brief compared to the overall training duration. They serve merely as necessary initialization steps to stabilize the learning environment. During these preliminary phases, performance metrics naturally fluctuate: the agent exhibits stable behavior during data collection (using the base policy) but experiences an inevitable “adaptation dip” during residual injection as the RL module explores. Detailed parameter settings for these phases are provided in Table 7. To provide a clear and fair comparison of the proposed methods (*Sparse World Imagination Reward* and *Dynamic Weight Scheduling*), we exclude these initialization artifacts from our results. The performance curves in Fig. 4 strictly record the *Main Training Phase*, starting immediately after the residual weight reaches its target value. This ensures the visualization focuses on the model’s convergence behavior and asymptotic performance rather than its setup dynamics.

Appendix D: Implementation Details

To ensure reproducibility, this appendix details the key configurations and hyperparameter settings used in the two training stages of the SC-VLA framework.

Stage I: SC-VLA Base Policy Training. The base policy is implemented using the DiT architecture from *GROOT N1.5*. We jointly optimize the flow-matching objective and the multimodal prediction heads using the AdamW optimizer. The model is trained for 50,000 iterations on a single NVIDIA L40 GPU. The detailed network configurations and training hyperparameters are summarized in Table 6.

Table 6. SC-VLA base model hyperparameter settings.

Hyperparameter	Value
Batch size	32
Training steps	50,000
Learning rate	1×10^{-4}
Model init seed	42
Optimizer	AdamW

Stage II: SC-VLA Residual Policy Training. In the second stage, the residual module is trained using the Soft Actor-Critic (SAC) algorithm. During this phase, the parameters of the base model are fully frozen, and optimization is performed exclusively on the residual network π_{res} .

To account for performance variance of the base policy across different tasks, we adopt a task-adaptive residual scaling strategy. Specifically, following an inverse-correlation principle, tasks for which the base model achieves higher success

rates are assigned smaller residual scaling and evaluation coefficients, enabling fine-grained refinement while preserving high-quality priors. Conversely, larger coefficients are used for tasks where the base policy performs worse, allowing for more substantial action corrections.

Although the residual scaling factor varies across tasks, we employ a consistent dynamic scheduling strategy for the predictive guidance reward across all experiments. Key hyperparameters used in the reinforcement learning stage are summarized in Table 7.

Table 7. SC-VLA residual model hyperparameter settings.

Tasks	Shared Parameters		Task-Specific Parameters	
	Hyperparameter	Value	Hyperparameter	Value
StackCube	Random seed	0	Total timesteps	500,000
	Replay buffer size	Total steps	Learning start steps	30,000
	Discount factor γ	0.97	Exploration steps	100,000
	Target smoothing τ	0.01	Residual scale (train)	0.01
	Batch size B	1024	Residual scale (eval)	0.005
PlaceSphere	Policy learning rate	1×10^{-4}	Total timesteps	500,000
	Critic learning rate	1×10^{-4}	Learning start steps	8,000
	Entropy coeff. α	0.2	Exploration steps	30,000
	Gradient clipping	50	Residual scale (train)	0.01
LiftPegUpright	Update-to-Data (UTD)	0.5	Residual scale (eval)	0.005
	Training frequency	64	Total timesteps	600,000
	Guide weight w_{guide}	0.6	Learning start steps	30,000
			Exploration steps	100,000
PegInsertion			Residual scale (train)	0.01
			Residual scale (eval)	0.005
			Total timesteps	3,000,000
			Learning start steps	60,000
		Exploration steps	200,000	
		Residual scale (train)	0.1	
		Residual scale (eval)	0.03	

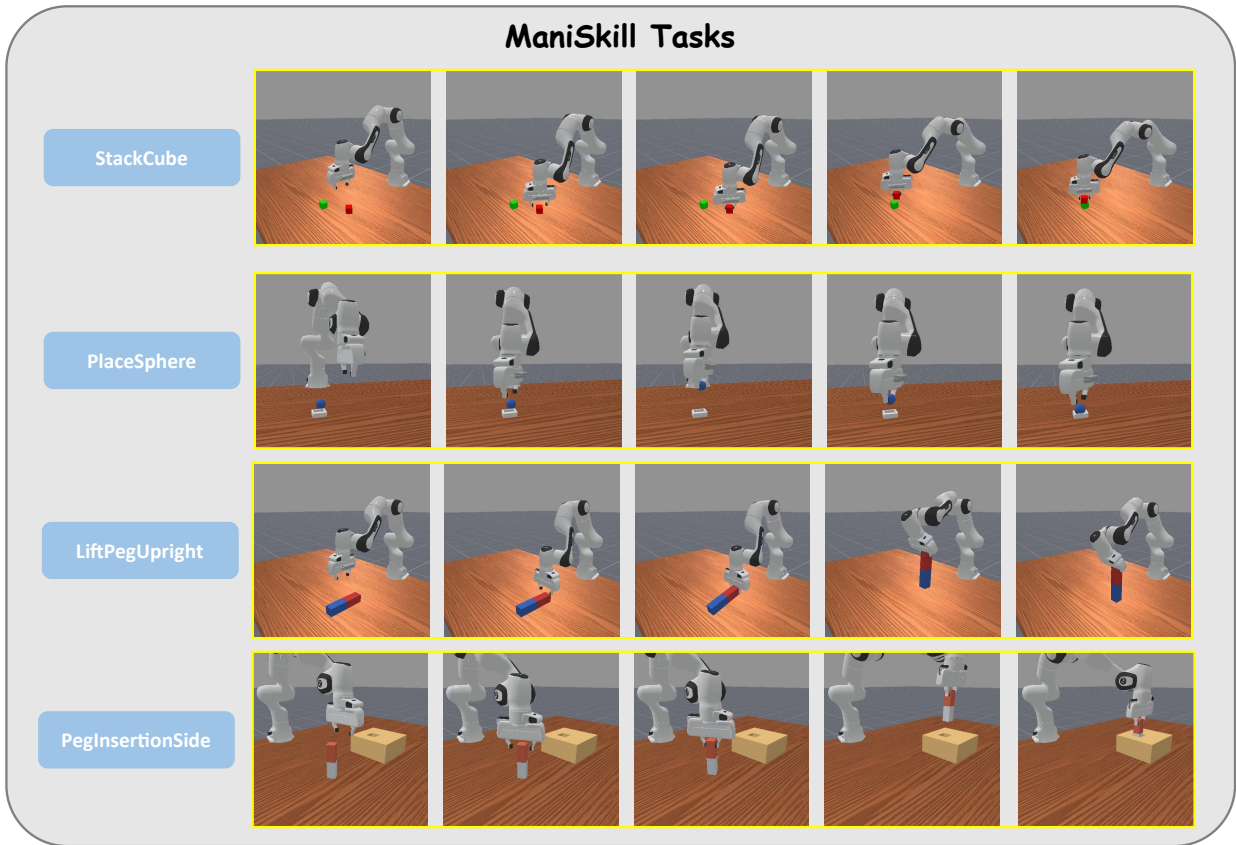


Figure 6. Visualization results of Maniskill simulated tasks.

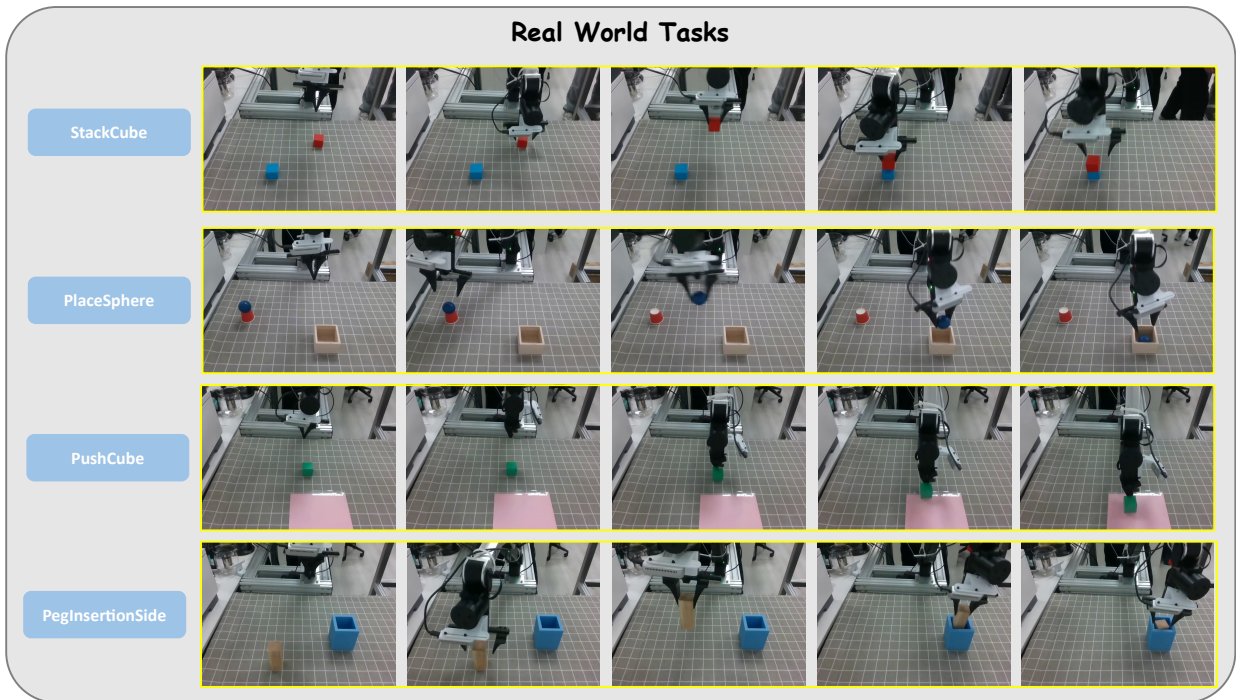


Figure 7. Visualization results of real-world tasks.